

Small Molecule and High Polymeric Phosphazenes Containing Oxypyridine Side Groups and Their Organometallic Derivatives: Useful Precursors for Metal Nanostructured Materials

Carlos Díaz* and Maria Luisa Valenzuela

Departamento de Química, Facultad de Ciencias, Universidad de Chile, Las Palmeras 3425, Santiago, Chile

Received July 7, 2005; Revised Manuscript Received October 14, 2005

ABSTRACT: The pyridine-containing copolymers $\{[\text{NP}(\text{O}_2\text{C}_{12}\text{H}_8)]_X[\text{NP}(\text{OC}_5\text{H}_4\text{N})_2]_{1-X}\}_n$, with $X = 0.7$ (**3a**) and $X = 0.8$ (**3b**), and their respective organometallic derivatives of approximate formula $\{[\text{NP}(\text{O}_2\text{C}_{12}\text{H}_8)]_X[\text{NP}(\text{OC}_5\text{H}_4\text{N}\cdot\text{MLn})_2]_{1-X}\}_n$ with $\text{MLn} = \text{CpFe}(\text{dppe})$, $\text{CpRu}(\text{PPh}_2)_2$, $(\eta^5\text{-CH}_3\text{C}_5\text{H}_4)\text{Mn}(\text{CO})_2$, and $\text{W}(\text{CO})_5$ have been prepared and characterized. As models, the simple compounds $\text{N}_3\text{P}_3(\text{OC}_6\text{H}_5)_5\text{OC}_5\text{H}_4\text{N}\cdot\text{W}(\text{CO})_5$ (**2**) and $\text{HOC}_5\text{H}_4\text{N}\cdot\text{W}(\text{CO})_5$ (**1**) have also been prepared and characterized. Pyrolysis of the organometallic polymers in air affords metallic nanostructured materials, which according to transmission electron microscopy (TEM), scanning electron microscopy (SEM), back-electron scattered imaging (BEI), energy-dispersive X-ray microanalysis, and micro-Raman data can be formulated as the coexistence of metal and metal oxide in the case of tungsten and as manganese phosphate salt in the case of manganese. A plausible formation mechanism is proposed, and the pyrolysis of the organometallic polyphosphazene polymer as a new and general method to obtain metallic nanostructured materials is discussed.

Introduction

Polymeric complexes are interesting for many reasons.¹ In particular, polymers having MLn organometallic fragments anchored to a polymeric chain may be useful in the design of new types of catalysts² and as precursors of preceramic materials.^{2,3} Although several organometallic derivatives of polyphosphazene polymers (see Chart 1) with $\text{L} = \text{PPh}_2$, $\text{CH}_2\text{-CN}$, and CN have been reported,^{4–10} few reports have appeared on polyphosphazene polymers with pyridine side groups.¹¹

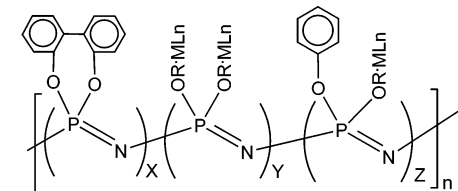
Most of the phosphazene pyridine complexes that have been characterized are cyclic models.^{13–16} This has been due in part to the scarcity of polyphosphazene–oxypyridine¹² as well as to the difficulty of obtaining their respective organometallic derivatives.¹¹

We have previously reported a series of organometallic polymers of the type $\{[\text{NP}(\text{O}_2\text{C}_{12}\text{H}_8)]_X[\text{NP}(\text{O}_6\text{H}_4\text{X}\cdot\text{MLn})_2]_{1-X}\}_n$ with $\text{X} = \text{CH}_2\text{CN}$,^{4,5,7,8} CN ,¹⁰ and PPh_2 ,^{6,9} and with $\text{MLn} = \text{CpFe}(\text{dppe})$, $\text{Cp}^*\text{Fe}(\text{dppe})$, $\text{CpRu}(\text{PPh}_2)_2$, $(\eta^5\text{-CH}_3\text{C}_5\text{H}_4)\text{Mn}(\text{CO})_2$, and $\text{W}(\text{CO})_5$. We have also found from thermal studies^{4–11} of such systems in N_2 that relatively high pyrolytic residues are obtained. The pyrolytic yields are dependent mainly on two factors: (i) the nature of the organometallic fragment and (ii) the nature of the spacer linking the organometallic fragment and the phosphorus chain.

With the purpose of comparing their thermal properties with those of systems having a pyridine spacer as well as different organometallic fragments, in this paper we report the synthesis, characterization, and thermal study of the series of organometallic copolymers **4–7** shown in Chart 2.

For comparison, we have also prepared the cyclic phosphazene model $\text{N}_3\text{P}_3(\text{OC}_6\text{H}_5)_5\text{OC}_5\text{H}_4\text{N}\cdot\text{W}(\text{CO})_5$ (**2**) as well as the simpler model $\text{HOC}_5\text{H}_4\text{N}\cdot\text{W}(\text{CO})_5$ (**1**). Pyrolysis of the tungsten and manganese containing polymers in air yields metallic nanoclusters of $\text{M}/\text{M}_n\text{O}_m$.

Chart 1

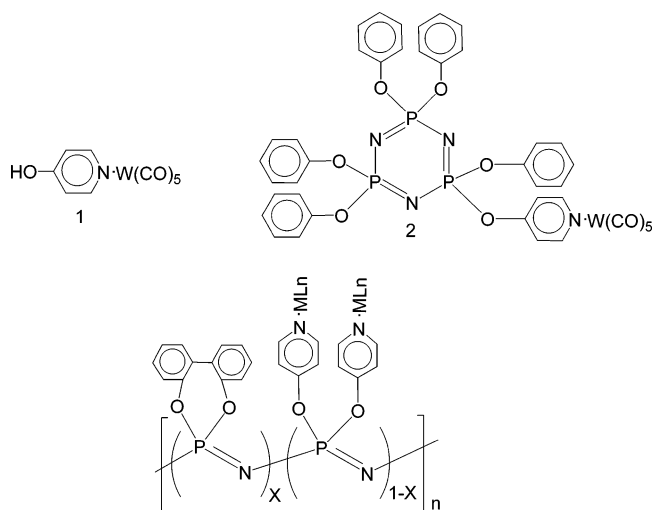


R	MLn	X	Y	Z	Ref
	$\text{CpFe}(\text{dppe})$	0.80	0.18	0.02	8
	$\text{CpFe}(\text{dppe})$	0.55	0.20	0.25	8
	$\text{CpRu}(\text{PPh}_3)_2$	0.80	0.18	0.02	8
	$\text{CpRu}(\text{PPh}_3)_2$	0.55	0.20	0.25	8
	$\text{Cr}(\text{CO})_5$	0.80	0.18	0.02	4
	$(\pi\text{-CH}_3\text{-C}_5\text{H}_4)\text{Mn}(\text{CO})_2$	0.55	0.20	0.25	5
	$\text{C}_5(\text{CH}_3)_5\text{Fe}(\text{dppe})$	0.80	0.18	0.02	7
	$(\pi\text{-CH}_3\text{-C}_5\text{H}_4)\text{Mn}(\text{CO})_2$	0.60	0.40	0.0	6
	$\text{W}(\text{CO})_5$	0.65	0.35	0.0	9

Materials with submicron dimensions like nanoparticles represent an exciting new class of materials.^{17a,b} As a consequence of their tiny size, nanomaterials often display unique physical and chemical properties that are not typical of the bulk materials. For instance, optical, magnetic, and electric properties are sensitive to size effects. Furthermore, nanosized particles are also very efficient in the field of catalysis^{17c,d} due to their high surface-to-volume ratio. Consequently, numerous processes for nanomaterials synthesis have been investigated attempting to control their size, morphology, structure, and chemical

* Corresponding author. E-mail: cdiaz@uchile.cl.

Chart 2



N°	X	1-X	MLn
3a	0.7	0.3	-----
3b	0.8	0.2	-----
4a	0.7	0.3	W(CO) ₅
4b	0.8	0.2	W(CO) ₅
5a	0.7	0.3	Mn(η^5 -CH ₃ -C ₅ H ₄)(CO) ₂
6a	0.7	0.3	Fe(η^5 -C ₅ H ₅)dppe
7a	0.7	0.3	Ru(η^5 -C ₅ H ₅)(PPh ₃) ₂

composition. Many studies have been published on the production of nanoparticles.¹⁷ There are two main routes for their preparation: chemical methods using the aqueous method or the sol-gel technique, among others, and physical methods using spray pyrolysis or vapor condensation methods, almost all of them in solution. Few solid-state methods for preparing metallic nanostructured materials have been reported. Manners et al. have prepared iron nanostructures from the solid-state pyrolysis of polymers containing iron and silicon of the type [Fe(η^5 -C₅H₅)₂ SiR'R']_n.^{2b-d} In this context a solid-phase pyrolytic method is an interesting alternative for making nanomaterials.

This paper also describes a new possible method for preparing structured nanomaterials using a pyrolysis-induced chemical transformation of an organometallic polyphosphazene precursor. By selecting an appropriate organometallic fragment, the desirable metallic nanostructured materials can be obtained.

Experimental Part

All reactions were carried out under dinitrogen using standard Schlenk techniques. IR spectra were recorded on an FT-IR Perkin-Elmer 2000 spectrophotometer. Micro-Raman spectra were obtained on a micro-Raman Renishaw Research Raman RM2000 microscope system equipped with a Leica microscope (DMLM series).

NMR spectra were recorded on a Bruker AC-300 instrument using CDCl₃ as solvent unless otherwise stated. ¹H and ¹³C{¹H} NMR are given in δ relative to TMS. ³¹P{¹H} are given in δ relative to external 85% aqueous H₃PO₄. Coupling constants are in hertz. GPC were measured on Perkin-Elmer equipment with a model LC 250 pump, a model LC 290 UV, and a model LC 30 refractive index detector. The samples were eluted with a 0.1 wt % solution of tetra-*n*-butylammonium bromide in THF through Perkin-Elmer PLGel (Guard, 10⁵, 10⁴, and 10³ Å) at 30 °C. Approximate molecular weight calibration was obtained using narrow molecular weight distribution polystyrene standards. Visible absorption spectra were measured on a UV-2450 Shimadzu instrument with a solid diffuse reflectance attachment. Thermogravimetric analysis (TGA) measurements were made with a Mettler

TA 4000 instrument. DSC thermograms were obtained with a Mettler 300 differential scanning calorimeter equipped with a TA 1100 computer. The polymer samples were heated at a rate of 10 °C/min from ambient temperature to 1000 °C under a constant nitrogen flow.

The metal analyses were performed at the Analytical Laboratory of the Departamento de Química, Facultad de Ciencias, Universidad de Chile. Digestion of the solid samples was carried out with a DK-20 heating digester, using 1:4 H₂SO₄:HNO₃ mixture under several continuous cycles. Determination of each metal was done spectrophotometrically as follows: iron as the sulfosalicylic acid complex, manganese as MnO₄²⁻, and ruthenium as its bathocuproinedisulfonic acid complex.

SEM photographs were taken with a Philips EM 300 microscope. Energy-dispersive X-ray microanalysis (EDAX) was performed on a NORAN Instrument microprobe attached to a JEOL 5410 scanning electron microscope.

TEM images were made on a JEOL SX100 transmission microscope. The finely powered samples were dispersed in water and dropped on a conventional carbon-washed copper grid.

The pyrolysis experiments were made by pouring weighed portions (0.05–0.15 g) of the organometallic polymers into aluminum oxide boats that were placed in a tubular furnace (Lindberg/Blue Oven model STF55346C-1) under an air flow, heating from 25 to 300 °C and then to 800 °C and annealing for 2 h. The heating rate was 10 °C/min under an air flow of 200 mL/min.

The ligand, HOC₅H₄N (Aldrich), the organometallic CpRu-(PPh₃)₂Cl, and (η^5 -CH₃C₅H₄)Mn(CO)₃ (Merck) were used as purchased. CpFe(dppe)I and W(CO)₅(MeOH) were prepared as reported previously.^{8,11}

Preparation of N₃P₃(OC₆H₅)₃OC₅H₄N. A mixture of N₃P₃(OC₆H₅)₃Cl¹⁸ (1.00 g, 1.57 mmol), HO-C₅H₄N (0.15 g, 1.57 mmol), K₂CO₃ (0.4347 g, 3.14 mmol), and [Bu₄N]Br (0.71 g, 2.20 mmol) was refluxed in acetone (40 mL) for 11 h. The solution was filtered through Celite and the solvent evaporated in a vacuum. The red oily residue was extracted with toluene to give a red solution. *n*-Hexane was added to obtain a light red oil, which was washed with *n*-hexane and dried under reduced pressure.

IR (KBr, pellets, cm⁻¹): 3060 w, 2962 m, 2875 m, 1698 w, 1637 w, 1590 s, 1487 vs, 1269 s, 1240 m, 1197 vs, 1179 vs, 1160 vs, 1070 m, 1024 m, 1007, 994 m, 953 s, 905 m, 892 m, 773 m, 734 m, 690 m, 585 m. ¹H NMR (CDCl₃): 8.38, 8.37 (*o*-H, OC₅H₄N), 7.1–6.91 (m, OC₆H₅), (*m*-H, OC₅H₄N) 8.84, 6.82. ¹³C NMR {¹H} (CDCl₃, ppm): 151.33, 129.4, 116.04 (OC₅H₄N), 151.33, 129.39, 124.82, 116.36 (P(OC₆H₅)). UV/vis(CH₂Cl₂): λ = 260 nm, 270 nm.

Anal. Calcd for C₃₅H₂₉O₆N₄P₃: C, 60.54; H, 4.17; N, 8.07. Found: C, 60.49; H, 4.25; N, 7.78.

Preparation of {[NP(O₂C₁₂H₈)]_x[NP(OC₅H₄N)₂]_{1-x}]_n. **General Procedure.** To a THF solution of [NP(Cl)₂]_n (100 mL, 4.46 g, 38.51 mmol for **3a**; 85 mL, 1.85 g, 0.016 mmol for **3b**) were added 2,2'-(*o*-HO)C₆H₄-C₆H₄(OH) (5.02 g, 26.96 mmol for **3a**; 2.09 g, 11.2 mmol for **3b**) and solid K₂CO₃ (21.29 g, 154.048 mmol for **3a**; 8.85 g, 64 mmol for **3b**), and the mixture was refluxed with mechanical stirring for 20 h for **3a** and 16.5 h for **3b**. For both preparations the ³¹P NMR showed two broad complex signals in the -4 to -8 ppm (**3a**) and -23 to -27 ppm (**3b**) regions, with 0.7/0.3 relative intensities for **3a** and 0.2/0.8 for **3b**. Then HOC₅H₄N (3.29 g, 38.51 mmol for **3a**; 0.063 g, 0.66 mmol for **3b**) and Cs₂-CO₃ (12.55 g, 38.51 mmol for **3a**; 0.21 g, 1.1 mmol for **3b**) were added, refluxing for another 20 h. The reaction mixture was poured in water to give a precipitate that was filtered and washed with water (2 × 100 mL). The precipitate was dissolved in THF concentrated until viscous and poured dropwise into water with stirring. The precipitated product was purified twice by dissolving in THF, concentrating the solution, and precipitating dropwise, first in 2-propanol and finally in hexane. The resulting lentil-shaped white powder was dried at 70 °C in a vacuum for 7 days. Yield: 30% for **3a** and 40% for **3b**.

Analysis and spectroscopic data: **3a** IR (KBr pellet, cm⁻¹): 3064 w, 3029 w, 2976 w, 2864, 1634 w, 1582 m, 1499 m, 1477 s, 1412

Table 1. Relevant Spectroscopic Data for the Oligomer Models and Their Polymers

compd	IR ^a				NMR ^b ³¹ P
	$\nu(\text{C-OP})$	$\nu(\text{PN})$	$\nu(\text{P-OC})$	$\nu(\text{OC}_5\text{H}_4\text{N})$	
1 ^c				1633, 1649, 1510	
2 ^d	1269	1197, 1179, 1161	1070	1637, 1590, 1487	8.55
3a	1268	1242, 1189	1094	1637, 1582, 1499	−5.79 to 23.77
3b	1268	1189, 1242	1189	1634, 1582, 1499	−4.72 to 24.5

^a KBr solid (cm^{−1}). ^b CDCl₃ solution (ppm). ^c **1**^c refers to compound **1** without the organometallic fragment, namely pyridine. Other IR data: $\nu(\text{OH}) = 3219 \text{ cm}^{-1}$. ^d **2**^d refers to compound **2** without the organometallic fragment, namely N₃P₃(OC₆H₅)₅(OC₅H₄N).

Table 2. Thermal Data for Polyphosphazenes **3a** and **3b** and Their Organometallic Derivatives **4a**, **4a**, **5a**, **6a**, and **7a**

polymer	temp dec ^a (°C)	% residue (at 800 °C)	T _g (°C)
3a	417	34	129
3b	470	37	156
4a	380	36	105
4b	370	60	73
5a	300	50	122
6a	370	30	<i>b</i>
7a	360	10	<i>b</i>

^a A small weigh loss was seen below 100 °C. ^b No T_g was seen.

s, 1393 s, 1369 m, 1268 vs, 1242 vs, 1189 vs, 1094 vs, 1048 m, 996 m, 923 vs, 890 vs, 825 m, 786 vs, 751 vs, 716 vs, 609 vs, 590. ¹H NMR (CDCl₃): 7.47 (o-H, OC₅H₄N), 7.22–6.8 (m, br, O₂C₁₂H₈). ¹³C NMR {¹H} (CDCl₃, ppm): 48.26, 129.1, 125.4, 122.16 (O₂C₁₂H₈), 150.78, 148.26, 115.76 (OC₅H₄N). Anal. Calcd for C_{11.4}H₈O₂N_{1.6}P: C, 59.43; H, 3.48; N, 9.73. Found: C, 60.4; H, 3.7; N, 8.4.

3b: IR (KBr, pellet, cm^{−1}): 3065 w, 3029 w, 2976 w, 2864 w, 1634 w, 1583 m, 1499 m, 1477 s, 1412 s, 1393 s, 1369 m, 1268 vs, 1242 vs, 1189 vs, 1093 vs, 1048 m, 997 m, 923 vs, 890 vs, 825 m, 786 vs, 752 vs, 716 vs, 609 vs, 590. ¹H NMR (CDCl₃): 7.90 (o-H, OC₅H₄N), 7.5–6.5 (m, br, O₂C₁₂H₈). ¹³C NMR {¹H} (CDCl₃, ppm): 148.44, 129.1, 125.24, 122.34 (O₂C₁₂H₈), 150.74, 148.44, 115.84 (OC₅H₄N). Anal. Calcd for C_{12.6}H₈O₂N_{1.4}P: C, 60.57; H, 3.48; N, 8.53. Found: C, 59.95; H, 4.0; N, 8.7.

Other relevant spectroscopic data are summarized in Table 1.

Preparation of the Organometallic Derivatives. Preparation of HOC₅H₄N·W(CO)₅. A mixture of HO-C₅H₄N (0.18 g, 1.92 mmol) and W(CO)₅(MeOH) (prepared by irradiating 0.65 g (1.92 mmol) of W(CO)₆ in methanol (130 mL) for 45 min) was stirred for 45 min at room temperature. The solvent was removed under reduced pressure and the yellow-oil residue washed twice with diethyl ether and dried under reduced pressure. Yield: 0.25 g, 49%. IR (KBr pellet, cm^{−1}): 3089 w, 2955 w, 2863 w, 2068 w, 1911 vs, 1873 vs, 1654 m, 1581 w, 1504 s, 1370 m, 1319 m, 1229 w, 1228 w, 1215 w, 1199 s, 1023 w, 840 m, 588 w. The ¹H NMR and ¹³C NMR data for the O-C₅H₄N group are given in Table 2. Other signals are: ¹³C NMR {¹H} (CDCl₃, ppm): 199, 191 W(CO)₅. Anal. Calcd for C₁₀H₄O₆NW: C, 28.66; H, 0.95; N, 3.34. Found: C, 27.80; H, 1.06; N, 4.34.

Preparation of N₃P₃(OC₆H₅)₅OC₅H₄N·W(CO)₅. A mixture of N₃P₃(O-C₆H₅)₅(O-C₅H₄N) (0.23 g, 0.31 mmol) and W(CO)₅(MeOH) (obtained by irradiation of 0.51 g of W(CO)₆ in 130 mL of methanol for 45 min) in methanol (20 mL) was stirred for 21 h at room temperature. The solvent was removed under reduced pressure, and the residue was extracted with CH₂Cl₂, filtered through Celite, and concentrated to ca. 10 mL. A 4:1 *n*-hexane/diethyl ether mixture was added, and the yellow powdered precipitate was washed twice with the same solvent mixture and dried under reduced pressure. Yield: 0.25 g, 49%. The ¹H NMR and ¹³C NMR data of the O-C₅H₄N group are given in Table 2. Other signals are: IR (KBr, pellet, cm^{−1}): 3070 w, 2964 w, 2919 w, 2071 w, 1923 vs, 1591 m, 1489 vs, 1269 m, 1246 m, 1198 vs, 1177 vs, 1161 vs, 1025 m, 1008 m, 951 vs, 906 m, 771 s, 729 m, 689 m, 584 m. ¹H NMR (CDCl₃, ppm): 7.28–7.13 (m OC₆H₅). ¹³C NMR {¹H} (CDCl₃, ppm): 151.3; 129.4, 120.99, 116.04 P(OC₆H₅), 193 W(CO)₅. Anal. Calcd for C₄₀H₂₉O₁₁N₄P₃W: C, 47.13; H, 2.84; N, 5.49. Found: C, 46.04; H, 5.10; N, 5.10.

Preparation of {[NP(O₂C₁₂H₈)]_x[NP(OC₅H₄N·MLn)₂]_{1-x}]_n. Preparation of Derivatives with W(CO)₅: General Procedure for **4a and **4b**.** A solution of W(CO)₅(MeOH) prepared by irradiation of 0.16 g, 0.47 mmol of W(CO)₆ for **4a** and 0.65 g, 2.01 mmol of W(CO)₆ for **4b** was stirred with a CH₂Cl₂ solution of 0.15 g, 0.47 mmol of polymer **3a** for **4a** and 0.18 g, 2.01 mmol of polymer **3b** for **4b**, for 8 h. The solvent was then evaporated under vacuum, and the precipitate was washed with diethyl ether to give blue-gray (**4a**) and light-green (**4b**) solids. Yields: **4a**, 60%; **4b**, 70%. IR (KBr pellet, cm^{−1}) (**4a**): 3063 w, 2962 w, 2066 w, 2017 w, 1972 s, 1716 vs, 1603 m, 1503 s, 1477 s, 1439 s, 1388 s, 1272 vs, 1245 vs, 1192 vs, 1095 vs, 1038 m, 1014 s, 941 vs, 914 vs, 917 vs, 785 s, 750 s, 716 s, 608 s, 589 m, 535 s. Anal. Calcd for C_{14.4}H₈O₅N_{1.6}PW_{0.6}: C, 40.97; H, 1.90; N, 4.65. Found: C, 40.42; H, 3.19; N, 3.93. UV/vis, λ_{max} (solid, nm) s = 425 (sh).

IR (KBr pellet, cm^{−1}) (**4b**): 3071 w, 2932 w, 2071 w, 1979 m, 1919 vs, 1721 w, 1633 m, 1605 m, 1499 m, 1477 m, 1379 m, 1247 vs, 1194 vs, 1096 m, 1025 w, 954 m, 787 m, 754 m, 717 w, 608 m, 589 m, 539 m. Anal. Calcd for C_{14.6}H₈O₄N_{1.4}PW_{0.4}: C, 47.17; H, 2.15; N, 5.28. Found: C, 28.91; H, 2.1; N, 5.45. Poor combustion of the sample gives a low carbon and nitrogen content. λ_{max} (solid, nm) = 420 (sh), 425 (sh).

Preparation of Derivative of (n⁵-CH₃C₅H₄)Mn(CO)₃ with {[NP(O₂C₁₂H₈)]_{0.7}[NP(OC₅H₄N)₂]_{0.3}]_n. A THF solution of {[NP(O₂C₁₂H₈)]_{0.7}[NP(OC₅H₄N)₂]_{0.3}]_n (0.69 g, 0.3 mmol) was added to a solution of (n⁵-CH₃C₅H₄)Mn(CO)₂THF (prepared by irradiating a THF solution of (n⁵-CH₃C₅H₄)Mn(CO)₃ (0.1 mL, 0.6 mmol)), and the mixture was stirred at room temperature for 2 h, when the solution became red in color and a red-brown solid was formed. The supernatant was removed by decantation, and the dark brown solid remaining was washed with *n*-hexane and dried in a vacuum.

IR (KBr pellet, cm^{−1}): 3061 m, 3031 m, 2919 w, 2851 w, 1656 w, 1589 w, 1477 s, 1289 w, 1243 s, 1190 s, 1118 s, 1094 s, 921 vs, 785 s, 750 vs, 715 m, 608 m, 590 m, 531 m.

Anal. Calcd for C_{14.42}H_{11.42}N_{1.6}O_{2.46}PMn_{0.23}: C, 59.71; H, 3.93; N, 7.72; Mn, 4.35; Found: C, 58.98; H, 4.18; N, 7.52; Mn, 1.85.

Preparation of the Derivative of CpFe(dppe)I with {[NP(O₂C₁₂H₈)]_{0.7}[NP(OC₅H₄N)₂]_{0.3}]_n. A mixture of the polymer (0.14 g, 0.62 mmol) and CpFe(dppe)I (0.12 g, 0.19 mmol) in dichloromethane (20 mL) in the presence of TIPF₆ (0.13 g) at room temperature was stirred for 48 h. The cloudy red-orange solution was filtered through Celite, and the solution evaporated under vacuum. The solid residue was washed twice with a 3:1 *n*-hexane/diethyl ether mixture, and the red power was dried under reduced pressure. Poor combustion of the sample afforded a low carbon content.

IR (KBr pellet, cm^{−1}): 3062 m, 3039 m, 2921 w, 2875 w, 1652 w, 1589 w, 1477 s, 1281 w, 1247 s, 1197 s, 1096 s, 848 s, 695 m, 608 m, 592 m, 556 m, 531 m.

Anal. Calcd for C₃₀H₂₆N_{1.6}O_{1.8}P_{2.8}Fe_{3.6}Fe_{0.6}: C, 57.51; H, 4.15; N, 3.57; Fe, 5.35. Found: C, 56.57; H, 4.45; N, 4.42; Fe, 3.67.

Preparation of the Derivative of CpRu(PPh₃)₂Cl with {[NP(O₂C₁₂H₈)]_{0.7}[NP(OC₅H₄N)₂]_{0.3}]_n. A solution of CpRu(PPh₃)₂Cl (0.12 g, 0.16 mmol) in CH₃OH was stirred with the polymer (0.13 g, 0.55 mmol) in the presence of NH₄PF₆ (0.054 g, 0.33 mmol) at room temperature for 4 h. The yellow-brown solid formed was filtered off, washed with a mixture of *n*-hexane/diethyl ether, and dried under reduced pressure. The yellow solution remaining after filtering the initial precipitate was confirmed to be unreacted CpRu(PPh₃)₂Cl. As found sometimes and as seen with other organome-

talic polymers,^{22,23} the poor analytical results obtained were probably due to incomplete combustion.

IR (KBr pellet, cm^{-1}): 3056 m, 3023 m, 2923 w, 2937 w, 1679 w, 1589 w, 1482 s, 1231 w, 1275 s, 1186 s, 1116 s, 844 s, 752 s, 712 s, 539 s.

Results and Discussion

Oligomers and Polyphosphazene Containing Oxypyridine.

The $\text{N}_3\text{P}_3(\text{OC}_6\text{H}_5)_5\text{OC}_5\text{H}_4\text{N}$ oligomer was prepared by reaction of $\text{N}_3\text{P}_3(\text{OC}_6\text{H}_5)_5\text{Cl}$ with $\text{HOC}_5\text{H}_4\text{N}$ in the presence of K_2CO_3 in acetone as solvent. As seen for other similar $\text{N}_3\text{P}_3(\text{OC}_6\text{H}_5)_{6-n}\text{L}_n$,^{13,14,18} the compound was obtained as an oil that solidified on standing in the freezer. Elemental analysis and spectroscopic data indicated that the compound is analytically pure (see Table 1 and Experimental Section).

The ^1H and ^{13}C NMR spectra show clearly the signals of the pyridine groups:^{11,16} 8.4 (d) ppm and 151.3, 129.5, and 116 ppm, respectively. On the other hand, the IR spectrum exhibits the typical pyridine bands corresponding to the CC and CN stretching modes of the $\text{C}_5\text{H}_4\text{N}$ ring¹¹ at 1637, 1590, and 1487 cm^{-1} . As found for other $\text{N}_3\text{P}_3(\text{OC}_6\text{H}_5)_{6-n}\text{L}_n$ systems,¹⁸ the ^{31}P NMR spectrum shows a single signal due to the similar electronic density of the six phosphorus atoms arising from the similar nature of the OC_6H_5 and the $\text{OC}_6\text{H}_5\text{X}$ (or $\text{OC}_5\text{H}_4\text{N}$) groups. Changes in the chemical environment on X are not noted by the phosphorus atom in the $\text{OC}_6\text{H}_5\text{X}$ units.

The $\{[\text{NP}(\text{O}_2\text{C}_{12}\text{H}_8)]_x[\text{NP}(\text{OC}_5\text{H}_4\text{N})_2]_{1-x}\}_n$ copolymers were prepared by the sequential reactions: (i) the $[\text{NPCl}_2]_n$ parents with 2,2'-dihydroxybiphenyl ($\text{HO}-\text{C}_6\text{H}_4-\text{C}_6\text{H}_4-\text{OH}$) and K_2CO_3 in THF to give the un-cross-linked linear polymer $\{[\text{NP}(\text{O}_2\text{C}_{12}\text{H}_8)]_x[\text{NPCl}_2]_{1-x}\}_n$ and (ii) addition of the 4-hydroxypyridine to complete the substitution of the chlorine atoms.¹¹ The average M_w measured by GPC were (**3a**) 696 000 (polydispersity ratio of 2.88) and (**3b**) 550 000 (polydispersity ratio of 3.4), which are analogous to those of other polyspirophosphazene copolymers containing the oxypyridine group.¹¹ All the analytical and spectroscopic data for these copolymers were in agreement with their formulas (see Table 1 and Experimental Section). As found for other similar polymers, the charge was confirmed by the ratio of the intensities of the ^{31}P NMR signals, IP_1/IP_2 , where IP_1 is the intensity of the phosphorus atoms of the $\text{P}-\text{O}_2\text{C}_{12}\text{H}_8$ unit and IP_2 is the intensity of the phosphorus atoms of the $\text{P}-\text{OC}_5\text{H}_4\text{N}$ unit.

The thermal stability of the copolymers was estimated by the TGA curves. The thermal data for these and other compounds are summarized in Table 2. Both copolymers showed a first mass loss of $\sim 2\%$ starting at around 100 $^\circ\text{C}$ due to depolymerization of the poly-THF retained by the polymeric matrix and evaporation of the resulting THF, followed by a fast loss centered at 417 $^\circ\text{C}$ (**3a**) and 470 $^\circ\text{C}$ (**3b**). After reaching 800 $^\circ\text{C}$, the residues were 34% for **3a** and 37% for **3b**. The final residues correspond to the cross-linked pyrolytic material formed during decomposition,¹⁹ as seen with other poly-(aryloxyphosphazene)s. The thermal stability allowed a study of the DSC curves from -50 to 250 $^\circ\text{C}$, which showed a well-defined glass transition with $T_g = 129$ $^\circ\text{C}$ and $\Delta C_p = 0.18$ $\text{J g}^{-1} \text{K}^{-1}$ for **3a** and 156 $^\circ\text{C}$ and $\Delta C_p = 0.14$ $\text{J g}^{-1} \text{K}^{-1}$ for **3b**. These T_g values are very high for a polyphosphazene and are consistent with the contribution of the rigid $[\text{NP}(\text{O}_2\text{C}_{12}\text{H}_8)]$ units.¹¹ However, since the value for the homopolymer $[\text{NP}(\text{O}_2\text{C}_{12}\text{H}_8)]_n$ is 160 $^\circ\text{C}$, it is apparent that the presence of the $[\text{NP}(\text{OC}_5\text{H}_4\text{N})]$ units makes a significant contribution to the T_g . In contrast, although the T_g for the $[\text{NP}(\text{OC}_5\text{H}_4\text{N})]_n$ homopolymer is not available, it is known that for the $[\text{NP}(\text{OC}_6\text{H}_4\text{X})]_n$ diphenoxyphosphazene homopolymers the T_g values vary

Table 3. NMR Data for the Dissociation Equilibrium $\text{XC}_5\text{H}_4\text{N}\cdot\text{W}(\text{CO})_5 \rightleftharpoons \text{XC}_5\text{H}_4\text{N} + \text{W}(\text{CO})_5$

X = OH						
	A	B	C	A'	B'	C'
^1H	8.47 8.45	6.79 6.78		7.71 7.69	6.64 6.62	
^{13}C	156.95	117.17	179.5	138.1	113.7	165.96
X = $\text{N}_3\text{P}_3(\text{OC}_6\text{H}_5)_5\text{O}$						
	A	B	C	A'	B'	C'
^1H	8.48 8.46	6.79 6.78		8.35 8.33		
^{31}P	8.83 ^a 8.46 ^b					
^{13}C	151.3	116.04		150.43	116.04	

a coordinate
b uncoordinate

between 33 and 111 $^\circ\text{C}$.¹⁹ The T_g values for copolymers **3a** and **3b** are therefore relatively close to those of polyspirophosphazene, in agreement with the small fraction of pyridine groups.

Organometallic Derivatives. $\text{HOC}_5\text{H}_4\text{N}\cdot\text{W}(\text{CO})_5$ Model. In agreement with Allcock's approximation,²⁰ and in order to facilitate the interpretation of the most complex polymeric systems, we have prepared the organometallic models $\text{N}_3\text{P}_3(\text{OC}_6\text{H}_5)_5\text{OC}_5\text{H}_4\text{N}\cdot\text{W}(\text{CO})_5$ (**2**) and $\text{HOC}_5\text{H}_4\text{N}\cdot\text{W}(\text{CO})_5$ (**1**). Reaction of 4-hydroxypyridine with the photochemically generated complex $[\text{W}(\text{HOMe})(\text{CO})_5]$ ¹¹ yielded compound $\text{HOC}_5\text{H}_4\text{N}\cdot\text{W}(\text{CO})_5$ as a yellow solid. The IR spectrum of compound **4** both as the solid (KBr) and in solution (CH_2Cl_2) made clearly evident the coordination of the $\text{W}(\text{CO})_5$ fragment (solid: $\nu(\text{CO})$ 2068 w, 1911 vs, 1873 m; solution: $\nu(\text{CO})$ 2055 w, 1928 vs, 1885 m, sh). Linking of the organometallic fragment to pyridine was also evident from the absence of the strong oxypyridine band ($\nu(\text{CC})$) at 1549 cm^{-1} and the appearance of a new band at 1581 cm^{-1} typical of oxypyridine coordination. In the NMR spectrum, of special significance was the effect on the o-H signals of the pyridine groups, which change from 7.89 ppm in free $\text{HOC}_5\text{H}_4\text{N}$ to 8.47 ppm upon coordination. However, and as found in other MLn systems, where L is a ligand containing pyridine,¹⁶ partial dissociation of the pyridine-metal bond occurred. In fact, other signals at 7.71 ppm corresponding to o-H of the uncoordinated 4-hydroxypyridine were seen. Consistent with this, in the ^{13}C NMR spectrum there are two sets of signals corresponding to the coordinated $\text{HOC}_5\text{H}_4\text{N}$, as shown in Table 3. Thus, an estimation of the equilibrium constant using the above NMR data gives $K_{\text{eq}} \approx 2.4$.

Thus, in the ^{13}C NMR spectrum the typical signals of the carbonyl groups of $\text{W}(\text{CO})_5$ coordinated to the oxypyridine nitrogen were found at 199 and 191 ppm. Other ^1H and ^{13}C signals were found in their normal positions (see Table 3 and Experimental Section). Coordination of the tungsten fragment was also evidenced by the UV-vis spectrum. The maximum at 420 nm is assigned to the $^1\text{A}_1 \rightarrow ^1\text{E}$ transition and is in good agreement with the absorption energy expected for the $\text{W}(\text{CO})_5$ chromophore linked to the nitrogen ligands.²¹

Table 4. Selected Spectroscopic Data and Thermal Values for the Organometallic Derivates of the Oligomer and Polymer Model

compd	IR (cm ⁻¹) ^a					NMR ³¹ P (ppm)
	$\nu(\text{C-OP})$	$\nu(\text{PN})$	$\nu(\text{P-OC})$	$\nu(\text{OC}_5\text{H}_4\text{N})$	$\nu(\text{MLn})$	
1				1635 1851 1404	2068 1911 1873	
2	1268	1197 1177 1161	1070	1637 1589 1487	2064 1908 1838	8.46 ^b
4a	1272	1192	1095	1716 1602 1584 1503	1974 1913	<i>c</i>
4b		1247 1195	1096	1719 1633 1604	2071 1977 1920	<i>c</i>
5a	1289	1243 1186	1118	1581 1589	2054 1951 1839	<i>c</i>
6a	1281	1247 1197	1095	1652 1589		<i>c</i>
7a	1231	1275 1186	1096	1116		<i>c</i>

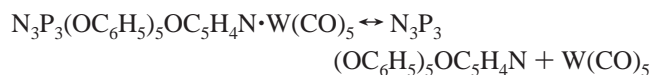
^a KBr solid. ^b CDCl₃ solution. ^c Insoluble sample.

N₃P₃(OC₆H₅)₅OC₅H₄N·W(CO)₅ (3) Model. Reaction of N₃P₃(OC₆H₅)₅OC₅H₄N with the photochemically generated complex [W(HOMe)(CO)₅] yielded the compound N₃P₃(OC₆H₅)₅OC₅H₄N·W(CO)₅ as a yellow solid. The IR spectrum of compound **3**, both as solid (KBr) and in solution (CH₂Cl₂), clearly showed the coordination of the W(CO)₅ fragment (solid: $\nu(\text{CO})$ 2064 w, 1908 vs, 1838 m; solution: $\nu(\text{CO})$ 2071 w, 1922 vs, 1880 m).

Bonding of the organometallic fragment to pyridine was also evident from the absence of the strong $\nu(\text{CC})$ oxypyridine band at 1589 cm⁻¹ and the appearance of a new band at 1592 cm⁻¹ typical of oxypyridine coordination. Other data are shown in Table 4.

Of special significance in the NMR spectrum was the effect on the o-H signals of the pyridinoxy groups, which changes from 8.38 ppm in N₃P₃(OC₆H₅)₅OC₅H₄N to 8.48 ppm in **2** upon coordination. In the ¹³C NMR spectrum a signal seen at 193 ppm was assigned to the carbonyl groups of W(CO)₅ coordinated to the oxypyridine nitrogen.¹⁶ Other ¹H and ¹³C signals were found to have their normal positions (see Table 3 and Experimental Section).

Thus, similarly to what has been found in other phosphazenes containing oxypyridine side groups,¹⁶ dissociation of the metal fragment occurred:



Using ³¹P NMR data, an equilibrium constant of $K = 6.4$ was estimated. As mentioned above, the $\nu(\text{CO})$ bands in CH₂Cl₂ solution are split compared to those of $\nu(\text{CO})$ in the solid state, suggesting the presence of two species: one containing the coordinated W(CO)₅ unit and the other one the free W(CO)₅. NMR data showing two sets of signals with similar chemical shift values are also in agreement with this, as shown in Table 2. Coordination of the tungsten fragment was also evidenced by the UV/vis spectrum. The maximum around 400 nm is assigned to the ¹A₁ → ¹E transition and agrees well with the absorption energy expected for the W(CO)₅ chromophore linked to the nitrogen ligands.²¹

Polymeric Complexes of {[NP(O₂C₁₂H₈)]_x[NP(OC₅H₄N)₂]_{1-x}]_n with [W(HOMe)(CO)₅]. Reaction in dichlo-

romethane solution of the copolyphosphazenes containing oxypyridine with the photochemically generated [W(HOMe)(CO)₅] yields slight soluble yellow to green solids. As seen with other organometallic polymer complexes,²² the product, initially soluble in the reaction mixture, became insoluble and did not redissolve in the solvents after precipitation with a diethyl ether/*n*-hexane mixture. Also, in the case of polymer **3b** a color change from yellow to green occurred after drying the solid under vacuum. We believe that cross-linking of the polyphosphazene occurred.²² Microanalysis and the IR and the UV/vis absorption spectra of both **3a** and **3b** were consistent with coordination of the available oxypyridine groups. In fact, the $\nu(\text{CN})$ band of the pyridine group seen around 1582 cm⁻¹ in both polymers disappears after coordination of the W(CO)₅ fragment, and new bands appear at 1603 cm⁻¹ for **4a** and 1605 cm⁻¹ for its homopolymer **4b**, characteristic of the coordination of pyridine groups with metal fragments, as seen in its models (see Table 4). The $\nu(\text{CO})$ bands of the W(CO)₅ fragment in the solid state (KBr) were also seen at 2017, 1972, and 1931 cm⁻¹ for **4a** and at 2071, 1977, and 1920 cm⁻¹ for **4b**. A weak band at 1718 cm⁻¹ was also seen, which was attributed to the presence of W(CO)₄ units linking polyphosphazene chains. This shows the proposed cross-linking mentioned above.

Other bands, such as $\nu(\text{PN})$, were found in their normal positions (see Table 4 and Experimental Section). The thermal properties of the organometallic polymers were investigated by TGA and DSC. For both polymers the final residue at 800 °C was greater than without the metal polymer (see Table 2), and this can be due to the contribution of the metal that may be involved in the ultimate cross-linking degradation process to form a pyrolytic material.^{22b}

The DSC curves for both polymers showed glass transition with $T_g = 105$ °C for **3a** and $T_g = 72.6$ °C for **3b**, both lower than those of the free oxypyridine polymer. This may be due to the enhancement of the flexibility of the P=N–P=N chains caused by the decreased steric effect of the aromatic ring in the polyspirophosphazenes due to the proximity of the organometallic groups.^{19,23}

Additional evidence of the formation of the polymeric W complexes comes from the diffuse reflectance UV/vis spectrum. Absorptions at 420 nm for **4a** and 410 and 445 nm for **4b**, typical of the W(CO)₅ chromophore,²¹ confirmed the presence of the metal in the polymer. Thus, the free oxypyridine-containing polyphosphazene does not absorb above 300 nm.

Complexes of {[NP(O₂C₁₂H₈)]_{0.7}[NP(OC₅H₄N)₂]_{0.3}]_n with CpFe(dppe)I, CpRu(PPh₂)₂Cl, and (n⁵-CH₃C₅H₄)Mn(CO)₃. Reaction of the {[NP(O₂C₁₂H₈)]_{0.7}[NP(OC₅H₄N)₂]_{0.3}]_n copolymer with (n⁵-CH₃C₅H₄)Mn(CO)₂THF (generated photochemically) yields an insoluble red-brown polymer whose elemental analysis is consistent with a 38% retention of the organometallic fragment. However, the percentage retention considering the metal analysis was somewhat smaller. As found for other organometallic derivatives of polyphosphazenes,^{22,23} some cross-linking is in agreement with their insolubility. The IR spectrum clearly indicated the presence of the polymer by the band at 1503 cm⁻¹ typical of the pyridine ring,¹¹ bands around 3056 and 1482 cm⁻¹ typical of O₂C₁₂H₈, and by the typical bands of the P=N bond at 1243 and 1186 cm⁻¹.

The presence of the organometallic fragment is evidenced by the bands at 2054, 1951, and 1839 cm⁻¹ assigned to the $\nu(\text{CO})$ characteristic of the Mn(CO)₂ moiety.⁵ Coordination of the organometallic fragment is also strongly confirmed by the appearance of a new weak band at 1620 cm⁻¹ characteristic of the coordination of organometallic groups through the nitrogen

atom in polyphosphazenes containing pyridine side spacers.¹¹

Additional evidence of the coordination of the ($n^5\text{-CH}_3\text{C}_5\text{H}_4$)-Mn(CO)₂ moiety arises from the solid-state UV/vis spectrum of the polymer. The free polymer does not show absorptions above 400 nm. The organometallic polymer has a broad absorption band with shoulders rather than maxima. Using a rough approximation, the maximum could be centered around 450 and 700 nm, absorptions typical of the ($n^5\text{-CH}_3\text{C}_5\text{H}_4$)Mn(CO)₂ chromophores.⁵

In the TGA curve of the organometallic polymer **5a**, an initial loss of ca. 10% weight was seen, as has also been found for other similar polyphosphazenes.^{5,7} This can be attributed to the loss of some organometallic residues.

The thermolysis pattern above ca. 300 °C shows a sudden loss of weight due to volatilization of the previously formed cyclophosphazenes. This process is in agreement with the endothermic peaks shown by the DSC curves at this temperature. The percentage of nonvolatile residue at 900 °C was 50%. This relatively high pyrolytic residue can be due to the cross-linking of the polymeric chains, as mentioned and discussed by Allcock.^{22b}

Reaction of the copolymer $\{[\text{NP}(\text{O}_2\text{C}_{12}\text{H}_8)]_{0.7}[\text{NP}(\text{OC}_5\text{H}_4\text{N})_2]_{0.3}\}_n$ with CpFe(dppe)I in dichloromethane and in the presence of TlPF₆ yields an insoluble red-brown polymer. As found for other organometallic polymers, poor combustion of the sample gave a low carbon content^{7,8} (see elemental analysis data in the Experimental Section). Elemental analysis was consistent with 68% metal retention. Cross-linking of the polymer is in agreement with its insolubility. The IR spectrum clearly indicated the presence of the polymer by the band at 1513 cm⁻¹ typical of the pyridine ring,¹¹ by bands around 3062 and 1477 cm⁻¹ typical of O₂C₁₂H₈, and by the characteristic $\nu(\text{P}=\text{N})$ at 1247 and 1186 cm⁻¹.

The incorporation of the organometallic moiety is evidenced by the C—H out-of-plane bending vibration of the phenyl group of the dppe ligand coordinated with the iron at 695 cm⁻¹⁸ and the $\nu(\text{PF}_6)$ band at 848 cm⁻¹. Coordination of the organometallic fragment is also strongly confirmed by the appearance of a new weak band at 1631 cm⁻¹, as mentioned previously.

Additional evidence of the coordination of the CpFe(dppe) moiety arises from the solid-state UV/vis spectrum of the polymer. In the visible region, the organometallic polymer shows a broad absorption band without maximum, with shoulders at 420 and 600 nm. These absorptions are characteristic of iron—pyridine complexes like [CpFe(dppe)NC₅H₅] PF₆.²⁴ The thermolysis pattern is similar to that of organometallic polymer **5a**, with a 30% residue at 800 °C. As usually seen with other organometallic polymers, no glass transition was detected for this polymer.

Reaction of the copolymer $\{[\text{NP}(\text{O}_2\text{C}_{12}\text{H}_8)]_{0.7}[\text{NP}(\text{OC}_5\text{H}_4\text{N})_2]_{0.3}\}_n$ with CpRu(PPh₃)₂Cl in CH₃OH in the presence of NH₄PF₆ yields an insoluble yellow-brown polymer. As in the case of other organometallic polymers, poor combustion of the sample gave a low carbon content (see elemental analysis data in the Experimental Section). Metal-based analyses suggest ca. 32% of metal retention. Cross-linking of the polymer is consistent with its insolubility. The IR spectrum clearly indicated the presence of the polymer by the band at 1482 cm⁻¹ typical of pyridine ring,¹¹ bands around 3052 and 1482 cm⁻¹ typical of O₂C₁₂H₈, and the characteristic $\nu(\text{P}=\text{N})$ band at 1275 and 1186 cm⁻¹. Incorporation of the organometallic moiety is evidenced by the C—H out-of-plane bending vibration of the phenyl group of the PPh₃ ligand coordinated to the iron at 695 cm⁻¹⁸ and the $\nu(\text{PF}_6)$ band at 844 cm⁻¹. Coordination of the

organometallic fragment is also confirmed by the appearance of a new weak band at 1679 cm⁻¹, characteristic of coordinated pyridine.

Additional evidence of the coordination of the CpRu(PPh₃)₂ moiety arises from the solid-state UV/vis spectrum of the polymer. As seen in other Ru complexes and polymer derivatives,⁸ the organometallic polymer shows a continuously decreasing absorption with a shoulder at ca. 500 nm.

The thermolysis pattern is similar to that of organometallic polymer **5a**, with a 10% residue at 800 °C. As usually seen with other organometallic polymers, no glass transition was detected for this polymer.

Pyrolysis of the Organometallic Derivatives of Polyphosphazenes. It is well-known that the introduction of metal or organometallic fragments promotes cross-linking rather than depolymerization.^{22b} This in turn could give a reasonable ceramic yield after pyrolysis. Comparing the percentages of pyrolytic residues of organometallic copolymers **4a**, **4b**, **5a**, **6a**, and **7a** with those of other spacers containing copolymers (see Chart 1), it can be concluded that in general the OC₅H₄N·MLn unit increases the percentage of pyrolytic residue with respect to those containing the OC₆H₄PPh₂·MLn or OC₆H₄CH₂CN·MLn unit. This may be due to the easier cross-linking of the chain containing pyridine spacers because the smaller pyridine group is less bulky. The dependence of the percentage of pyrolytic residue on the metal points to the order W > Mn > Fe > Ru, but this series follows a different order for the nitrile copolymer: Mn > Ru > Fe.

The relatively large residues found in the thermal studies of the organometallic polymers under N₂ encourage us to study their pyrolysis in air. The pyrolysis of the organometallic polymers **4a**, **4b**, and **5a** in air was carried out in a tube furnace at 800 °C for 3 h. The resulting ceramics were white solids. SEM-EDAX and BEI studies carried out on a sample of the ceramic products showed them to be homogeneous for **4a** but heterogeneous for **4b** and **5a**. EDAX showed the preceramic materials to contain tungsten in **4a** and **4b** and manganese in preceramic **5a**. The presence of phosphorus and oxygen in variable amounts was seen in all the pyrolyzed polymers. In some cases small amounts of carbon and nitrogen were also found. Typical EDAX analyses of pyrolytic materials from polymers **4a**, **4b**, and **5a** are shown in Figure 1. Figure 1a shows the EDAX for the pyrolytic residue of polymer **4a**. Similar EDAX spectra were obtained for various different zones of the material. Figure 1b,c shows the EDAX analysis of two different zones of the material arising from pyrolysis of **4b**, with different spectra clearly indicating the inhomogeneity of the sample. Figure 1d shows the EDAX analysis of the pyrolytic residue obtained from the manganese polymer **5a**. Similar spectra were obtained for various different zones of the material.

For the pyrolysis product from **4b** the EDAX analysis shows slightly different percentages of W, O, and P. As seen in Figure 1b,c, two zones can be distinguished. Zone 1 shows the highest W content, approximately in agreement with a mixture of WO₃/W⁰. Zone 2 (Figure 1c) shows a lower W, than the sample in zone 1, with percentages in agreement with an approximate formula WP₂O₃.

IR and micro-Raman spectra of the pyrolytic residues from polymers **4a**, **4b**, and **5a** have very simple and similar patterns showing the presence of phosphorus oxides and some weak bands assigned to the metal oxides. Thus, the micro-Raman spectrum of the pyrolytic residue from polymer **4a** is identical to that of WO₃. EDAX analysis of the pyrolytic residue from polymer **4a** is consistent with WO₃ with an unprecedented

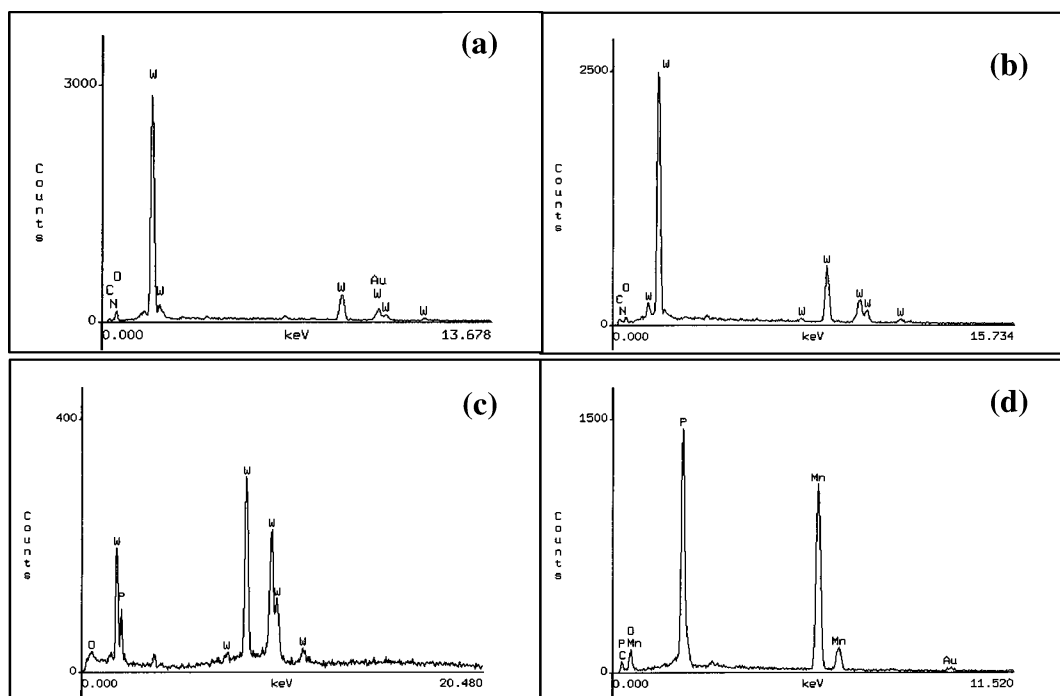
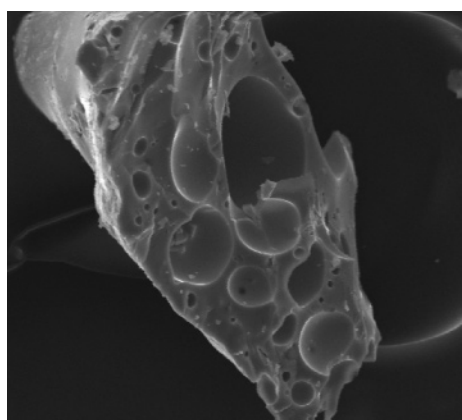
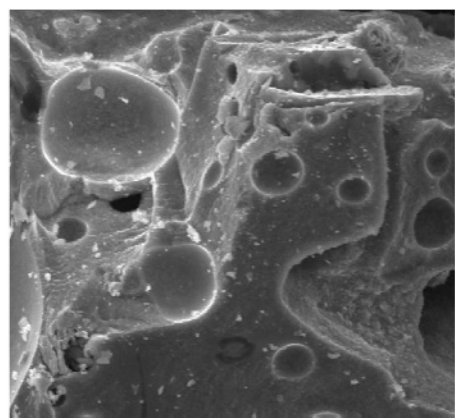


Figure 1. EDAX analyses for the pyrolytic residue of organometallic polymers **4a** (a), **4b** (b, c), and **5a** (d).



10 μm (a)



10 μm (b)

Figure 2. SEM micrographs of pyrolysis residues from organometallic polymers **4a** (a) and **4b** (b).

“gruyere cheese” type morphology, as shown in Figure 2a, while that of the pyrolytic residue from organometallic polymer **4b** shows the formation of a mixture of WO_3 —with a morphology

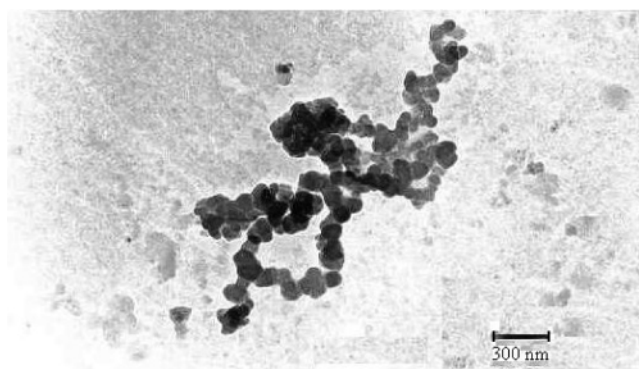


Figure 3. TEM image of pyrolysis residue from organometallic polymer **5a**.

similar to that of the pyrolytic residue from **4a**—and nanoporous metallic tungsten, as is shown in Figure 2b, for the pyrolytic residue from polymer **4b**.

On the other hand, for the residue from the pyrolysis of **5a**, EDAX analysis (shown in Figure 1d) and SEM are consistent with the formation of a nanostructured material with an approximate composition of MnPO .

The TEM image of this material (Figure 3) is similar to that of typical nanocomposites formed by inorganic metallic nanoparticles and organic polymers.²⁵ Nanoparticles of about 90 nm were seen.

Tungsten oxide is of interest in the field of photochromism^{26a,b} and as a source for the preparation of nanostructured WS_2 ^{26c} as devices for gas sensors^{26d,e} and as catalysts.^{26a,f,g} Several methods for obtaining nanostructured WO_3 in solution have been reported,²⁷ but to our knowledge no solid-state methods have been mentioned. On the other hand, nanostructured metallic W is not easy to obtain because of the high temperatures required for the conventional evaporation/condensation methods.²⁸ The preparation of nanostructured WO_3 and W by pyrolysis of the organometallic polymer provides of a simple method for obtaining these types of materials. More detailed studies with other metals and other polymers with other spacers are under way.

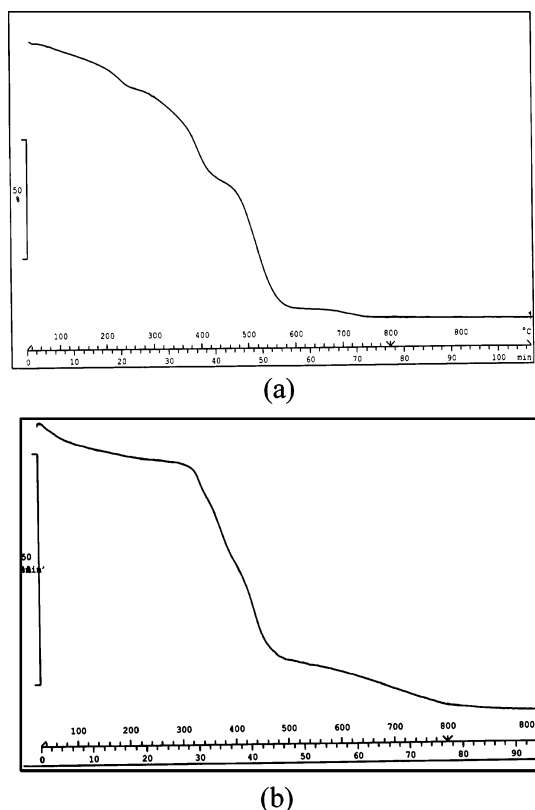


Figure 4. TGA curve for pyrolysis residue from organometallic polymer **4b** in air (a) and in N_2 (b).

Possible Formation Mechanism of the Metallic Nanostructures. Some insight into the mechanism of formation of the metallic nanostructures from the pyrolysis in air of the organometallic polymers can be obtained from the TGA curve of polymer **4b** in air, shown in Figure 4a, and in N_2 , shown in Figure 4b.

The first small weight loss in Figure 4a (8.4%) can be attributed to a solvent loss. The second largest weight loss was assigned to the loss of carbonyl groups from $W(CO)_5$ (calculated 14.77; found 15.57). The final weight loss can be attributed to the loss of CO_2 from the carbonization of the organic matter as well as to the loss of nitrogen and phosphorus oxides. The final residue was consistent with the formation of WO_3 (calculated 65.39%; found 66.6%). In agreement with this, the TGA curve in N_2 is different from that in air. The TGA curves in N_2 for some organometallic derivatives of polyphosphazenes have been discussed.^{4–9} In common with the TGA in air, some gradual weight loss until 200 °C is due to the loss of solvent molecules as well as to CO dissociation of the W atom. The most prominent weight loss near 350 °C has been ascribed to the volatilization of the previously formed cyclophosphazenes.

From this, the formation of the nanostructure from the organometallic polyphosphazenes can be thought (although somewhat speculatively) to occur in the following steps: (i) loss of CO; (ii) calcination of the organic matter, producing holes in the polymeric matrix, causing the agglomeration of the metallic particles; and (iii) oxidation of the metals to give metal oxides or formation of the $MnPO$.

Some of the advantages of this method for preparing metallic nanostructures are the following: (i) The inorganic metal atoms can be distributed uniformly—at the molecular level—along the macromolecular chains. (ii) The holes—formed by segregation of the organic moieties upon pyrolysis—act as templates for the growth of the nanoparticles. Then, by choosing different organic

spacers in the polymeric chain, the size of the holes may be modulated and the size of the nanoparticles can be controlled. (iii) The diversity in the chemical composition of the organometallic fragments (different metals, auxiliary ligands, electron density, etc.) should make it possible to obtain nanostructured materials with predetermined properties, such as catalytic (Ru, Pt, Au organometallic fragments), magnetic (Fe, Co organometallic fragments), energy storage (Ti organometallic fragments), etc.

Conclusions

1. Both the nature of the metal and the nature of the OC_6H_4X organic polymer spacer influence the yield of pyrolytic residues under N_2 for the organometallic polymer studied. For the metals, the order was $W > Mn > Fe > Ru$, while the side spacer with pyridine donor groups yields bigger pyrolytic residues than those containing benzylcyanide and phosphine spacers.

2. Pyrolysis in air gives lower yields than in N_2 due to the formation of metal/metal oxides nanostructures immersed in a matrix of phosphorus oxides.

3. It seems that the polyphosphazene polymers act as suitable solid-state templates and in some cases also as sources, of phosphorus oxides, which can be precursors of metal-phosphates that would lead to the formation of metallic nanostructures. This could be a novel and suitable general method for obtaining solid-state metallic nanostructures, especially in the case of the formation of nanostructured metal phosphate compounds. To our knowledge, no general methods in the solid state have been reported to produce metal-phosphate nanoparticles. Pyrolysis experiments with other polyphosphazenes containing anchored organometallic fragments are under way.

Acknowledgment. The authors acknowledge the financial support of Fondecyt (Project 1030515).

Supporting Information Available: IR spectrum of **2** in (a) CH_2Cl_2 solution and (b) solid-state (KBr pellet). This material is available free of charge via the Internet at <http://pubs.acs.org>.

References and Notes

- (1) Ciardelli, F.; Tsuchida, E.; Wöhrle, D. *Macromolecule-Metal Complexes*; Springer: Berlin, 1996.
- (2) (a) Garoou, P. E.; Gates, B. C.; Sherrington, D. C.; Hodge, P., Eds.; *Synthesis and Separation Using Functional Polymers*; Wiley: New York, 1988. (b) MacLachlan, M. J.; Ginzburg, M.; Coombs, N.; Coyle, T. W.; Raju, N. P.; Greedan, J. E.; Ozin, G. A.; Manners, I. *Science* **2000**, 287, 1460. (c) Manners, I. J. *Polym. Sci., Part A* **2002**, 40, 179. (d) Petersen, R.; Foucher, D. A.; Tang, B. Z.; Lough, A.; Raju, N. P.; Greedan, J. E.; Manners, I. *Chem. Mater.* **1995**, 7, 2045.
- (3) Pittman, C. U.; Wilkinson, G.; Stone, F. G. A.; Abel, E. W., Eds.; *Polymer Supported Catalysts Comprehensive Organometallic Chemistry*, 1st ed.; Pergamon Press: London, 1982; Vol. 8, Chapter 55, p 553 ff.
- (4) Díaz, C.; Castillo, P. J. *Inorg. Organomet. Polym.* **2001**, 11, 183.
- (5) Díaz, C.; Castillo, P.; Carriedo, G. A.; García Alonso, F. J.; Gómez-Elipe, P. *Macromol. Chem. Phys.* **2002**, 203, 1912.
- (6) Carriedo, G. A.; García Alonso, F. J.; González, P. A.; Díaz, C.; Yutronic, N. *Polyhedron* **2002**, 21, 2579.
- (7) Díaz, C.; Castillo, P. *Polym. Bull. (Berlin)* **2003**, 50, 12.
- (8) Díaz, C.; Valenzuela, M. L.; Barbosa, M. *Mater. Res. Bull.* **2004**, 39, 9.
- (9) Carriedo, G. A.; García Alonso, F. J.; González, P. A.; Gómez-Elipe, P. *Polyhedron* **1999**, 18, 2853.
- (10) Carriedo, G. A.; García-Alonso, F. J.; Gómez-Elipe, P.; Díaz, C.; Yutronic, N. *J. Chilean Chem. Soc.* **2003**, 48, 25–28.
- (11) (a) Carriedo, G. A.; García-Alonso, F. J.; García Álvarez, J. L.; Díaz, C.; Yutronic, N. *Polyhedron* **2002**, 21, 2587. (b) Diefenbach, U.; Allcock, H. R. *Inorg. Chem.* **1994**, 33, 4562. (c) Gleria, M.; De Jaeger,

- R., Eds.; *Applicative Aspects of Cyclophosphazenes*; Diefenbach, U. *Phosphazenes with Pyridine Groups*; Nova Sci. Publ., Inc.: Commack, NY, 2004.
- (12) Cho, Y.; Baek, H.; Sohn, Y. S. *Macromolecules* **1999**, *32*, 2167.
- (13) Chandrasekhar, V.; Justin, K. K. R. *J. Appl. Organomet. Chem.* **1993**, *7*, 1.
- (14) Chandrasekhar, V.; Negendran, S. *Chem. Soc. Rev.* **2001**, *30*, 193.
- (15) Carriedo, G. A.; Gómez Elipe, P.; García Alonso, F. J.; Fernandez Catuxo, L.; Díaz, M. R.; García Granda, S. *J. Organomet. Chem.* **1995**, *498*, 207.
- (16) Carriedo, G. A.; García Alonso, F. J.; García, J. L.; Carbajo, R. J.; López Ortiz, F. *Eur. J. Inorg. Chem.* **1999**, 1015.
- (17) (a) Edelstein, A. S.; Cammarata, R. C., Eds.; *Nanomaterials: Synthesis Properties and Applications*; J.W. Arrowsmith Ltd.: Bristol, 2000. (b) Klabunde, K. J. *Nanoscale Materials in Chemistry*; Wiley-Interscience: New York, 2001. (c) Grunes, J.; Gabor, J.; Somorjai, A. *Chem. Commun.* **2003**, 2257. (d) Bell, A. T. *Science* **2003**, *299*, 1688.
- (18) Díaz, C.; Barbosa, M.; Godoy, Z. *Polyhedron* **2004**, *23*, 1027 and references therein.
- (19) Gleria, M.; De Jaeger, R., Eds.; *Phosphazene: A Worldwide Insight*, F.J. Nova Sci. Publ., Inc.: Commack, NY, 2003; Chapter 8, pp 171–178.
- (20) (a) Allcock, H. R.; Al-Shali, S.; Ngo, D. C.; Visscher, K. V.; Parvez, M. *J. Chem. Soc., Dalton Trans.* **1996**, 3549. (b) Allcock, H. R.; Al-Shali, S.; Ngo, D. C.; Visscher, V. K.; Parvez, M. *J. Chem. Soc., Dalton Trans.* **1996**, 3521. (c) Allcock, H. R. *Acc. Chem. Res.* **1979**, *12*, 351.
- (21) Díaz, C.; Yutronic, N. *Polyhedron* **1987**, *6*, 503.
- (22) (a) Allcock, H. R.; Lavin, K. D.; Tollefson, N. M.; Evans, T. L. *Organometallics* **1983**, *2*, 267. (b) Allcock, H. R. *Chem. Mater.* **1994**, *6*, 1476.
- (23) (a) Allcock, H. R.; Nelson, C. J.; Coggio, W. D. *Chem. Mater.* **1994**, *6*, 516. (b) Allcock, H. R.; Connolly, J. T.; Sisco, S.; Al-Shali, S. *Macromolecules* **1988**, *21*, 323.
- (24) Díaz, C.; Arancibia, A. *Polyhedron* **1994**, *6*, 1476.
- (25) Gangopadhyay, R.; De, A. *Mater. Chem.* **2000**, *12*, 608.
- (26) (a) Sun, M.; Xu, N.; Cao, Y. W.; Yao, J. N.; Wang, E. G. *J. Mater. Res.* **2000**, *15*, 927. (b) Li, S. T.; El-Shall, M. S. *Nanostruct. Mater.* **1999**, *12*, 731. (c) Margolin, A.; Rosentsveig, R.; Albu-Yaron, R.; Popovitz-Biro, R.; Tenne, R. *J. Mater. Chem.* **2004**, *14*, 617. (d) Hoel, A.; Reyes, L. F.; Heszler, P.; Lantto, V.; Granqvist, C. G. *Curr. Appl. Phys.* **2004**, *4*, 547. (e) Hoel, A.; Ederth, J.; Kopniczy, J.; Hesler, P.; Kish, L. B.; Olsson, E.; Granqvist, C. G. *Smart Mater. Struct.* **2002**, *11*, 640. (f) Kang, Z. C.; Wang, Z. L. *J. Mol. Catal. A* **1997**, *118*, 215. (g) Shchukin, D. G.; Dong, W. F.; Sukhorukov, G. B. *Macromol. Rapid Commun.* **2003**, *24*, 462.
- (27) (a) Santato, C.; Odziemkowski, M.; Ulmann, M.; Augustynski, J. *J. Am. Chem. Soc.* **2001**, *123*, 10639. (b) Li, S. T.; El-Shall, M. S. *Appl. Surf. Sci.* **1998**, *129*, 330. (c) Li, S. T.; Germanenko, I. N.; El-Shall, M. S. *J. Cluster Sci.* **1999**, *10*, 533.
- (28) Magnusson, M. H.; Deppert, K.; Malm, J. O. *J. Mater. Res.* **2000**, *15*, 1564.

MA051480N